3152 *Chem. Mater.* **2010,** *22,* 3152–3157
DOI:10.1021/cm1001576

CHEMISTRY OF MATERIALS
Article

Thermally Stable, Silica-Doped ε-WO_3 for Sensing of Acetone in the Human Breath

M. Righettoni, A. Tricoli, and S.E. Pratsinis*

Particle Technology Laboratory, Institute of Process Engineering, Department of Mechanical and Process Engineering, Swiss Federal Institute of Technology, ETH Zurich, CH-8092 Zurich, Switzerland

Received January 18, 2010. Revised Manuscript Received March 23, 2010

Acetone in the human breath is a key marker for noninvasive diagnosis of diabetes. Here, sensing films of pure and SiO_2-doped WO_3 nanoparticles have been made, directly deposited and in situ annealed onto interdigitated electrodes by scalable flame aerosol technology. A unique innovation here is that these films consist of ε-WO_3, a metastable phase that has a high selectivity to acetone. The effect of nontoxic Si doping on the ε-phase content and crystal and grain sizes was investigated and correlated to the acetone sensing performance of these films. The thermal stability of these materials was characterized as well, revealing a unique opportunity for reliable sensing of acetone and noninvasive diagnostics of diabetes. An optimal doping level with 10 mol % SiO_2 resulted in highly sensitive and highly selective acetone sensors down to 20 ppb.

Introduction

Human breath analysis is an emerging field of medical diagnostics that promises rapid, noninvasive monitoring and even detection of illnesses.[1] Among hundreds of components in the human breath,[2] some gases are related to specific diseases and can be utilized as breath markers.[3] Acetone, in particular, is related to type 1 diabetes,[2,4] and its concentration increases from 300 to 900 ppb for healthy humans[5] to more than 1800 ppb for diabetic patients.[6] Accurate and rapid detection of such small concentration differences in the breath requires highly sensitive and highly selective analysis methods.[7]

Chemoresistive gas sensors made of nanostructured metal-oxide semiconductors offer a promising alternative[8−11] to more sophisticated systems (e.g., PTR-MS,[12] SIFT-MS[13]). Such sensors offer a lower limit of detection (LOD) in parts-per-billion concentrations to most reducing or oxidizing analytes[14] and can be miniaturized[15] and integrated in micro gas sensor systems[16] at low cost.[14,17] Major shortcomings, however, are their poor selectivity and long-term stability.[14] Lately, the latter has been improved by cosynthesis with other oxides, leading to thermally stable and highly sensitive nanoparticle layers.[18] For some analytes the selectivity is improved by formation of specific crystal planes and phases[11,17] that greatly facilitate the reliable detection of certain breath markers.

Among such materials, screen-printed δ-WO_3 thick films have been successfully applied to the measurement of low concentrations of acetone vapor (25−100 ppm).[19] Nanoparticles of γ-WO_3 with controlled size exhibiting high absorption capability have been made by evaporation−condensation of bulk tungsten oxide particles using a flame spray process.[20] Recently, the ferroelectric ε-phase of WO_3 captured during its flame synthesis has shown promising results for the selective and quantitative detection of acetone in parts-per-billion concentrations that is of critical importance in noninvasive diagnosis of diabetes by human breath analysis.[11] The spontaneous electric

*Corresponding author. E-mail: pratsinis@ptl.mavt.ethz.ch.

(1) Miekisch, W.; Schubert, J. K.; Noeldge-Schomburg, G. F. E. *Clin. Chim. Acta* **2004**, *347*, 25–39.
(2) Cao, W. Q.; Duan, Y. X. *Clin. Chem.* **2006**, *52*, 800–811.
(3) Manolis, A. *Clin. Chem.* **1983**, *29*, 5–15.
(4) Henderson, M. J.; Karger, B. A.; Wrenshall, G. A. *Diabetes* **1952**, *1*, 188–193.
(5) Diskin, A. M.; Spanel, P.; Smith, D. *Physiol. Meas.* **2003**, *24*, 107–119.
(6) Deng, C. H.; Zhang, J.; Yu, X. F.; Zhang, W.; Zhang, X. M. *J. Chromatogr., B* **2004**, *810*, 269–275.
(7) Cao, W. Q.; Duan, Y. X. *Crit. Rev. Anal. Chem.* **2007**, *37*, 3–13.
(8) Fleischer, M.; Simon, E.; Rumpel, E.; Ulmer, H.; Harbeck, M.; Wandel, M.; Fietzek, C.; Weimar, U.; Meixner, H. *Sens. Actuators, B* **2002**, *83*, 245–249.
(9) Natale, C. D.; Macagnano, A.; Martinelli, E.; Paolesse, R.; D'Arcangelo, G.; Roscioni, C.; Finazzi-Agro, A.; D'Amico, A. *Biosens. Bioelectron.* **2003**, *18*, 1209–1218.
(10) Ryabtsev, S. V.; Shaposhnick, A. V.; Lukin, A. N.; Domashevskaya, E. P. *Sens. Actuators, B* **1999**, *59*, 26–29.
(11) Wang, L.; Teleki, A.; Pratsinis, S. E.; Gouma, P. I. *Chem. Mater.* **2008**, *20*, 4794–4796.
(12) Hansel, A.; Jordan, A.; Holzinger, R.; Prazeller, P.; Vogel, W.; Lindinger, W. *Int. J. Mass Spectom. Ion Process.* **1995**, *149*, 609–619.
(13) Smith, D.; Spanel, P. *Rapid Commun. Mass Spectrom.* **1996**, *10*, 1183–1198.
(14) Eranna, G.; Joshi, B. C.; Runthala, D. P.; Gupta, R. P. *Crit. Rev. Solid State Mater. Sci.* **2004**, *29*, 111–188.
(15) Tricoli, A.; Graf, M.; Mayer, F.; Kuhne, S.; Hierlemann, A.; Pratsinis, S. E. *Adv. Mater.* **2008**, *20*, 3005–3010.
(16) Graf, M.; Barrettino, D.; Taschini, S.; Hagleitner, C.; Hierlemann, A.; Baltes, H. *Anal. Chem.* **2004**, *76*, 4437–4445.
(17) Korotcenkov, G. *Sens. Actuator B-Chem.* **2005**, *107*, 209–232.
(18) Tricoli, A.; Graf, M.; Pratsinis, S. E. *Adv. Funct. Mater.* **2008**, *18*, 1969–1976.
(19) Khadayate, R. S.; Sali, V.; Patil, P. P. *Talanta* **2007**, *72*, 1077–1081.
(20) Hidayat, D.; Purwanto, A.; Wang, W.-N.; Okuyama, K. *Mater. Res. Bull.* **2010**, *45*, 165–173.

Published on Web 04/23/2010

dipole moment[21] of ε-WO_3 leads to enhanced interaction with analytes having high dipole moment (e.g., acetone).[11] The ε-phase of WO_3 that is usually made by rapid solidification and is thermally stable only below −40 °C was made recently by scalable flame spray pyrolysis (FSP) of ammonium tungstate hydrate solutions.[11] Its further thermal stabilization at the operation temperatures (> 300 °C) of metal-oxide gas sensors required, however, doping with Cr that can be toxic.[22,23] Furthermore, Cr-doping increases the grain size[11] and thus somehow decreases the WO_3 sensitivity.[24] Alternatively to such heavy metal doping, phase stabilization is possible also by cosynthesis of WO_3 with light metal oxides such as SiO_2 that inhibits grain and sinter neck growth of metal oxide (e.g., TiO_2,[25] SnO_2,[18] WO_3[26]) nanoparticles and may even lead to drastically increased sensitivity.[18]

Here, sensing films of pure and SiO_2-doped WO_3 nanoparticles have been made by FSP, direct deposition and in situ flame annealing.[15] The effect of Si doping on the ε-phase content and crystal and grain sizes was characterized and correlated to the acetone sensing performance of these films. The thermal stability of these Si-doped ε-WO_3 nanoparticles was characterized up to 600 °C revealing a unique opportunity for optimal doping with SiO_2 and reliable sensing of acetone at the parts per billion level.

Experimental Section

Synthesis. A flame spray pyrolysis (FSP) reactor was used in combination with a water-cooled substrate holder as described in detail elsewhere[27] for synthesis and direct deposition of pure and SiO_2-doped WO_3 nanoparticle layers onto Al_2O_3 substrates featuring a set of interdigitated gold electrodes and a sensing area of 1 cm^2. These layers were mechanically stabilized by in situ annealing with a xylene-fed spray flame.[15] Sensing nanoparticles were prepared as follows: ammonium (meta)tungstate hydrate (Aldrich, purity >97%) and hexametyldisiloxane (HMDSO, Aldrich, purity >99%) were mixed, as dictated by the final SiO_2 content (0−40 mol %), and diluted in a 1:1 (volume ratio) mixture of diethylene glycol monobutyl ether (Fluka, purity >98.5%) and ethanol (Fluka, purity >99.5%) with a total metal (Si and W) concentration of 0.2 M. This solution was supplied at a rate of 5×10^{-3} L/min through the FSP nozzle and dispersed to a fine spray with 3−8 L/min oxygen (pressure drop 1.5 bar). That spray was ignited by a supporting ring-shaped premixed methane/oxygen flame (CH_4 = 1.25 L/min, O_2 = 3.2 L/min). An additional 5 L/min sheath oxygen was supplied from an annulus surrounding that flame to ensure excess oxidant flow.

Powder samples were collected with a vacuum pump (Vacuumbrand, RE 16) on a water-cooled glass-fiber filter (GF/D Whatman, 257 mm diameter) 50 cm above the burner, downstream of the Al_2O_3 substrate. The nozzle-substrate (NS) distance was 20 cm. The as-deposited films were stabilized in situ by increasing their adhesion and cohesion without crystal growth.[15] The substrate holder was lowered to NS = 14 cm and a particle-free (no metal precursor) spray flame fed with 12×10^{-3} L/min xylene and dispersed by 5 L/min O_2 (with another 5 L/min sheath O_2)[15] was impinged onto the film for 30 s. The supporting flame gas flow rates were those used during FSP deposition.

Particle Characterization. X-ray diffraction patterns were obtained by a Bruker, AXS D8 Advance diffractometer operated at 40 kV, 40 mA at 2θ (Cu Kα) = 10 - 60°, step = 0.04° and scan speed = 0.8°/min. The crystal size (d_{XRD}) was determined using the Rietveld fundamental parameter method with the structural parameters of monoclinic γ- and ε-WO_3.[28,29] The powder specific surface area (SSA) was measured by BET analysis using a Micromeritics Tristar 3000. The BET equivalent diameter was calculated using the density of WO_3 (7.16 g/cm^3) and SiO_2 (2.19 g/cm^3) for the nominal powder composition. Transmission electron microscopy was conducted in a Hitachi H600, operated at 100 kV. The morphology, patterning characteristics and thickness of the deposited layers were investigated by SEM with a LEO 1530 Gemini (Zeiss/LEO, Oberkochen) and a Tecnai F30 microscope (FEI (Eindhoven); field emission cathode, operated at 2 kV). Raman scattering spectra were recorded by a Renishaw InVia Raman microscope with a 514 nm laser with 25 mW power at a range of 280−1200 cm^{-1} with an exposure time of 10 s. For thermal analysis, the powders were annealed in an oven (Carbolite) in air for 5 h at 325−600 °C.

Sensor Characterization. Prior to sensing tests, all sensors were kept in air at 500 °C for 5 h to thermally stabilize them and avoid sintering and crystal/grain growth during analyte sensing at lower temperatures, which could lead to drifting. The sensor measurements were performed as described in detail elsewhere,[30] as it has been done even for breath analysis.[31] A wet diluted stream was generated by bubbling synthetic air through distilled water maintained at T_B = 20 °C (p_s = 23.38 mbar) to avoid condensation in the tube. The analyte mixture was acetone (10 ppm in synthetic air, Pan Gas 5.0) and ethanol (10 ppm in synthetic air, Pan Gas 5.0) in synthetic air. The gases were diluted further in synthetic air to reach the desired analyte concentration (20 to 3000 ppb). The sensors were placed in a quartz tube (3.5 cm in diameter and 35 cm long) located in a tubular furnace (Nabertherm) and connected to a voltmeter (Keithley, 2700 Multimeter/Data acquisition system) to measure the film resistance The operating temperature was varied between 325 and 500 °C and measured with a n-type thermocouple placed above the sensor. Other setups such as in situ heated sensors will give a different but quantitatively consistent sensor response.[15] The sensor response (S) is:

$$S = R_{air}/R_{analyte} - 1$$

where R_{air} is the film resistance in air with a given rh and $R_{analyte}$ is the film resistance with a given concentration of acetone or ethanol at the same rh. The sensor response was fairly reproducible with a maximum variation of ±9% between 100 and 600 ppb acetone.

(21) Woodward, P. M.; Sleight, A. W.; Vogt, T. *J. Solid State Chem.* **1997**, *131*, 9–17.
(22) Cohen, M. D.; Kargacin, B.; Klein, C. B.; Costa, M. *Crit. Rev. Toxicol.* **1993**, *23*, 255–281.
(23) Vonburg, R.; Liu, D. *J. Appl. Toxicol.* **1993**, *13*, 225–230.
(24) Xu, C.; Tamaki, J.; Miura, N.; Yamazoe, N. *Sens. Actuators, B* **1991**, *3*, 147–155.
(25) Akhtar, M. K.; Pratsinis, S. E.; Mastrangelo, S. V. R. *J. Am. Ceram. Soc.* **1992**, *75*, 3408–3416.
(26) Wang, X. S.; Sakai, G.; Shimanoe, K.; Miura, N.; Yamazoe, N. *Sens. Actuators, B* **1997**, *45*, 141–146.
(27) Madler, L.; Roessler, A.; Pratsinis, S. E.; Sahm, T.; Gurlo, A.; Barsan, N.; Weimar, U. *Sens. Actuators, B* **2006**, *114*, 283–295.
(28) Salje, E. *Ferroelectrics* **1976**, *12*, 215–217.
(29) Tanisaki, S. *J. Phys. Soc. Jpn.* **1960**, *15*, 573–581.
(30) Teleki, A.; Pratsinis, S. E.; Kalyanasundaram, K.; Gouma, P. I. *Sens. Actuators, B* **2006**, *119*, 683–690.
(31) Peng, G.; Tisch, U.; Adams, O.; Hakim, M.; Shehada, N.; Broza, Y. Y.; Billan, S.; Abdah-Bortnyak, R.; Kuten, A.; Haick, H. *Nat. Nanotechnol.* **2009**, *4*, 669–673.

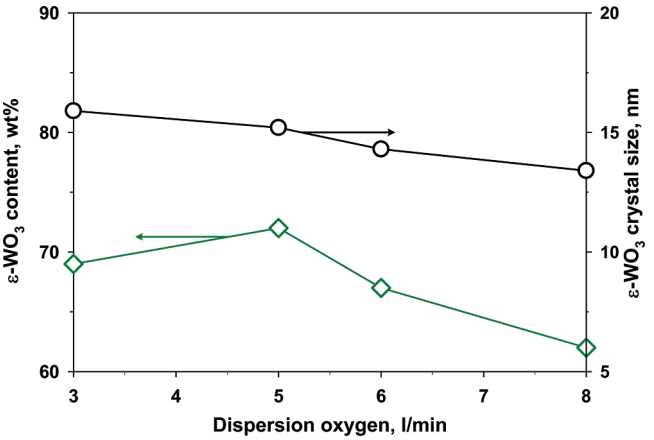

Figure 1. The ε-WO_3 phase content (diamonds) and crystal size (circles) as a function of dispersion oxygen flow during synthesis of WO_3 nanoparticles by flame spray pyrolysis of appropriate precursor solutions.

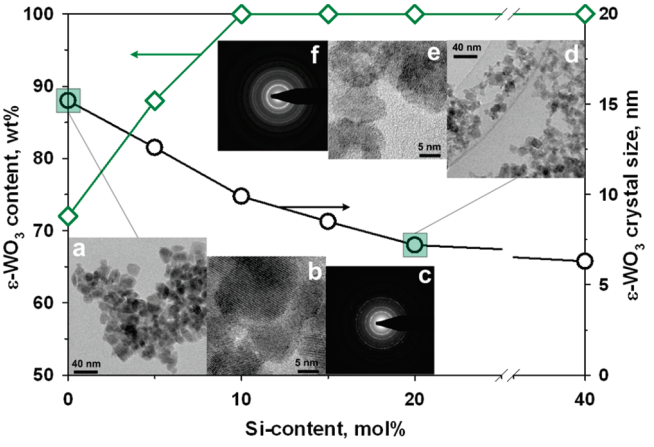

Figure 2. The ε-WO_3 phase content (diamonds) and crystal size (circles) as a function of Si doping of flame-made WO_3-based nanoparticles along with TEM images and electron diffraction (ED) patterns of (a−c) pure and (d−f) 20 mol % Si-doped WO_3 particles. Capture of 100 wt % acetone-selective ε-WO_3 phase is achieved by flame synthesis at 10 mol % Si doping.

Results and Discussion

The as-prepared, pure ε-WO_3 content and crystal size varied from 72 to 63 wt % (diamonds) and from 16 to 14 nm (circles), respectively, by varying the dispersion oxygen flow-rate from 3 to 8 L/min (Figure 1). This is in fair agreement with prior FSP synthesis of pure WO_3 (~13 nm)[11] and other oxides[27,30] as well as in the range of such nanoparticles made by evaporation−condensation of bulk WO_3 particles[20] of average initial size of about 700 nm in a spray flame. Here, all WO_3-based particles were made with 5 L/min O_2 feed through the FSP unit that gave the highest ε-WO_3 phase content (Figure 1).

Increasing the Si content from 0 to 40 mol % reduced the WO_3 crystal (Figure 2, circles) and grain sizes from 15.2 and 13 to 6.3 and 9.6 nm, respectively. This corresponds to an increase in specific surface area (SSA) from 64 to 117 m^2/g as confirmed also by TEM and ED analysis (Figure 2a−f). At 20 mol % Si, the particle size (Figure 2d,e) is smaller than that of pure WO_3 (a,b). Despite this high Si content, the ED analysis (Figure 2f) confirms the presence of smaller crystallites than those of pure WO_3 (c, bright spots). In fact, the crystal plane of pure WO_3 (Figure 2b) extends continuously and regularly through several particles, whereas at 20 mol % Si content, smaller WO_3 crystallites confined by amorphous SiO_2 regions (Figure 2e) are visible.

X-ray diffraction (XRD) analysis of as-prepared, pure WO_3 nanoparticles collected downstream of the sensor substrate revealed only the presence of γ- and ε-WO_3 phases (Figure 3) consistent with Wang et al.[11] Silica-doping increased the ε-phase content (Figure 2, diamonds) from 72 wt % for pure WO_3 to 100 wt % at 10 mol % Si. This is attributed to formation of an interstitial Si-WO_3 solid solution similar to Si doping of TiO_2 that interstitially stabilized the anatase phase instead of the thermodynamically dictated rutile.[25] In fact, incorporation of Si in the lattice could promote formation of the acentric ε-phase[28] instead of the more symmetric γ-phase.[29] In comparison, as-prepared WO_3 nanoparticles made by evaporation−condensation of larger WO_3 particles with a flame spray process[20] consisted of pure γ-WO_3. This is attributed, most probably, to the longer high-temperature particle residence time in such enclosed reactors than in the present open FSP ones, as observed[30] with flame synthesis of anatase and rutile TiO_2 favoring there the formation of the thermodynamically dictated rutile phase.

The thermal stability of pure and Si-doped WO_3 particles was investigated by annealing them in air for 5 h at 325−600 °C. Figure 3 shows the thermal evolution of the XRD spectra for (a) pure and (b) 20 mol % Si-doped WO_3 indicating that Si doping successfully stabilizes the ε-phase up to 500 °C. At 600 °C, pure WO_3 exhibits only the diffraction peaks of the γ-WO_3 crystallites[29] while the 20% Si-doped ones (Figure 4a, square) preserves up to 20 wt % of ε-WO_3. More in detail, the ε-phase content of as-prepared, pure WO_3 nanoparticles (Figure 4a, circles) decreases from 72 to 26 wt %, after annealing at 500 °C, whereas the 10 mol % Si-doped WO_3 decreases from 100 to only 87 wt %. A similar behavior is observed for the 15 (Figure 4a, triangles) and 20 (diamonds) mol % Si-doped WO_3.

The rapid reduction of the ε-phase content for all Si-doped WO_3 at 600 °C could be attributed to the higher diffusivity of W and/or oxygen, observed here, than that of other oxides (e.g., SnO_2).[18] In fact, even if 20 mol % Si doping stabilizes the ε-phase crystals around 20 nm up to 600 °C (Figure 4b, open diamonds), the γ-phase crystals (filled diamonds) grow to 69.5 nm, which is nearly the same (69.9 nm) to that of γ-crystallites of pure WO_3 at 600 °C (Figure 4b, filled circles). Similar sintering and phase transformation was observed for the 10 and 15 mol % Si content WO_3 samples (not shown). The ED patterns (inset Figure 4b) show that pure WO_3 sinters into large crystallites (bright spots) at 600 °C, while the Si-doped ones forms much fewer. This is in agreement with TEM analysis of these samples (Figure 5). Pure WO_3 (Figure 5a) forms large crystallites and sintering necks. In contrast, the 20 mol % Si-doped WO_3 forms amorphous SiO_2 domains, inhibiting the growth of WO_3 grain boundaries

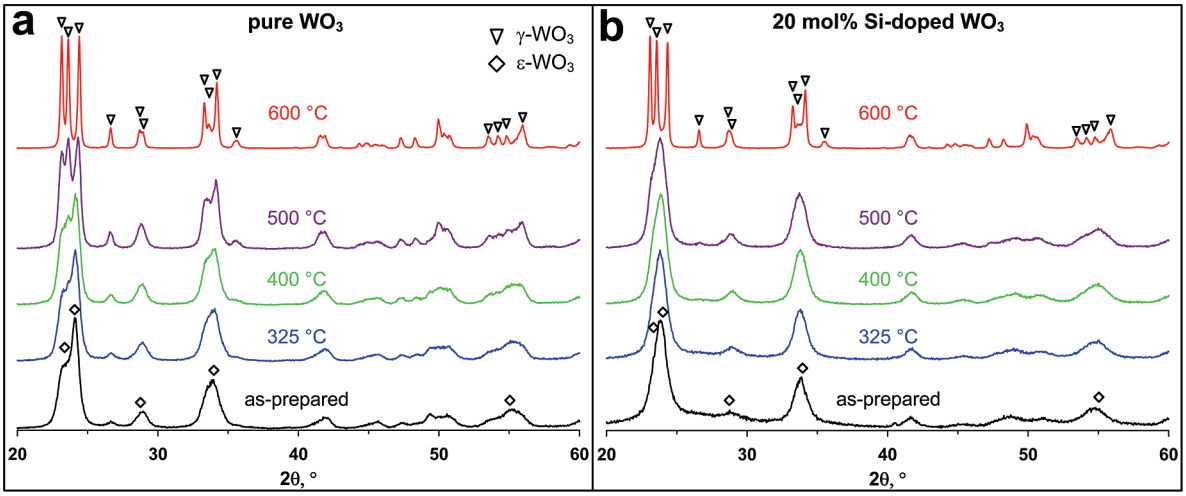

Figure 3. XRD patterns of (a) pure and (b) 20 mol % Si-doped WO_3 nanoparticles at different annealing temperatures (325−600 °C for 5 h in air). With increasing annealing temperature, the characteristic peaks of γ-WO_3 are visible already at 325 °C for pure WO_3 and only at 600 °C for the Si-doped WO_3.

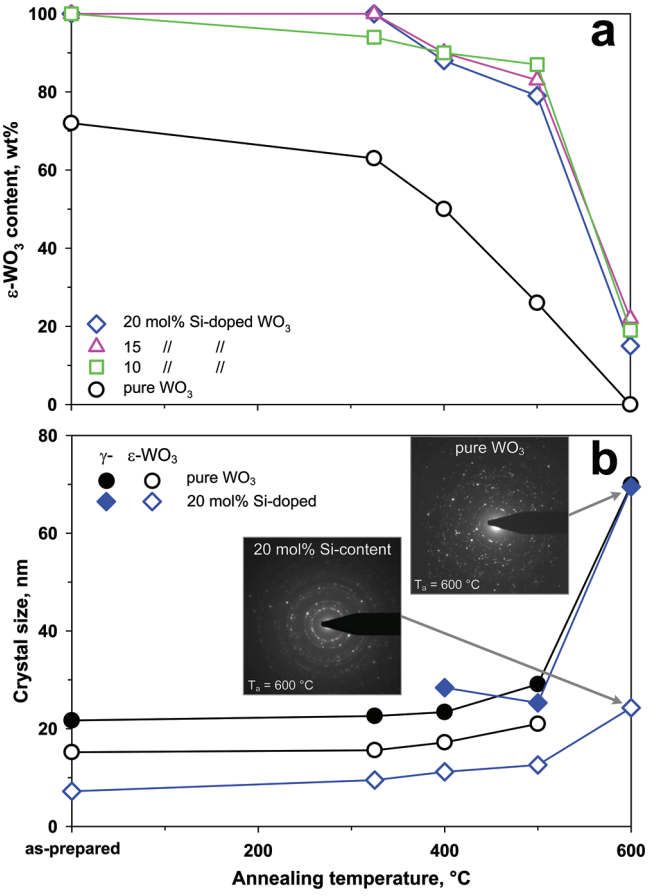

Figure 4. (a) ε-WO_3 phase content as a function of annealing temperature for 5 h in air for pure and Si-doped WO_3. (b) Crystal size (d_{XRD}) of pure (circles) and 20 mol % Si-doped (diamonds) WO_3 as a function of annealing temperature. Inset shows ED patterns of pure and 20 mol % Si-doped WO_3 after annealing at 600 °C for 5 h.

(Figure 5b,c,d) as observed[18] for SnO_2. However, some large particles are formed also at 20 mol % Si content WO_3, suggesting localized γ-phase transformation (Figure 5b).

Figure 6 shows the corresponding Raman spectra of (a) pure and (b) 20 mol % Si-doped WO_3 as a function of annealing temperature. The peaks at 324, 715, and

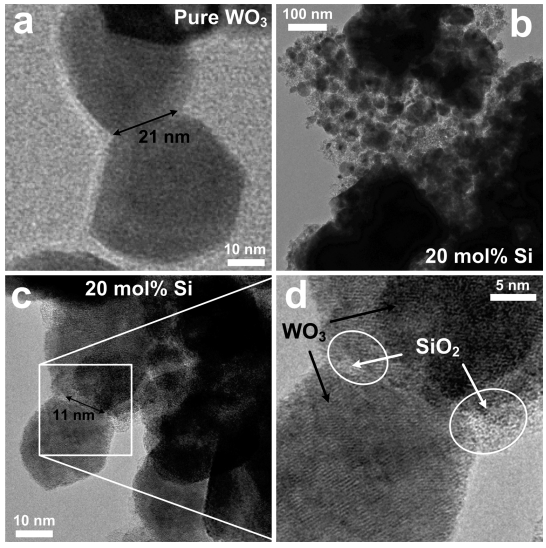

Figure 5. TEM images of (a) pure and (b−d) 20 mol % Si-doped WO_3 at different magnifications after annealing at 600 °C for 5 h in air. Neck growth between WO_3 nanoparticles is inhibited by Si doping (c,d).

805 cm^{-1} belong to the γ-WO_3 (space group: $P2_1/n$)[32] while those at 303, 370, 425, 642, 688, and 805 cm^{-1} belong to the acentric ε-phase (space group: Pc).[33] The weak peak at 942 cm^{-1} (Figure 6a, as-prepared) is assigned to the stretching mode of terminal W=O bond indicating surface tungsten hydrates.[32] The thermal evolution of the pure WO_3 Raman spectra (Figure 6a) confirms that the transformation from ε- to γ-phase advances rapidly already at low temperatures (≤325 °C). In contrast, at 20 mol % Si content, the ε-phase (Figure 6b) is stabilized up to 500 °C as it is shown by the peak at 688 cm^{-1}. The Raman spectra of the pure and Si-doped samples are identical at 600 °C confirming further the formation of the thermodynamically dictated γ-WO_3 at high temperatures (> 500 °C).

(32) Daniel, M. F.; Desbat, B.; Lassegues, J. C.; Gerand, B.; Figlarz, M. *J. Solid State Chem.* **1987**, *67*, 235–247.
(33) Arai, M.; Hayashi, S.; Yamamoto, K.; Kim, S. S. *Solid State Commun.* **1990**, *75*, 613–616.

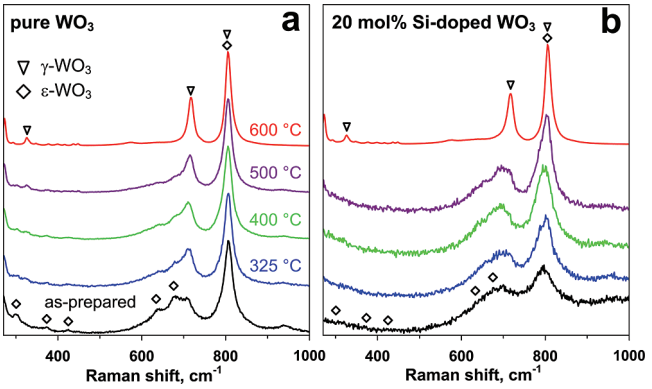

Figure 6. Raman spectra of (a) pure and (b) 20 mol % Si-doped WO_3 at different annealing temperatures for 5 h in air.

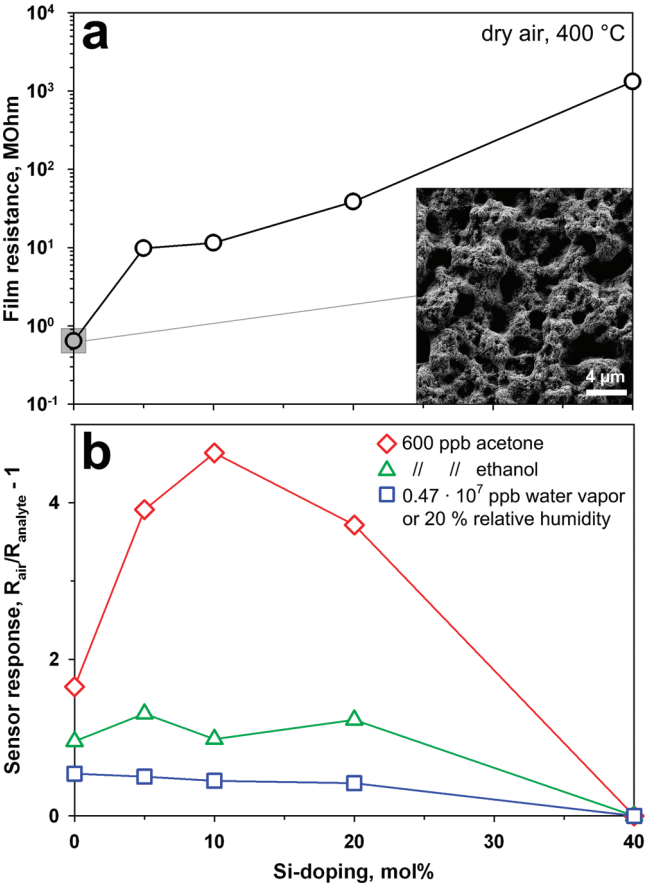

Figure 7. (a) Increasing the Si doping of WO_3 increases the resistance of the corresponding films. The inset shows the morphology of a pure WO_3 film after in situ annealing. (b) Response of WO_3-based sensors to 600 ppb acetone (diamonds) or ethanol (triangles) and 20% relative humidity (or 0.47×10^7 ppb) water vapor (squares) as a function of their Si content. A maximum sensor response and selectivity is found for such sensors doped with 10 mol % Si content.

Figure 7a shows the resistance in dry air (baseline) at 400 °C of films (inset) made by direct deposition and in situ annealing[15] of pure and Si-doped nanoparticles onto sensor substrates. The sensor baseline (Figure 7a) increases steeply by 4 orders of magnitude with increasing SiO_2 content from 0 to 40 mol %. This is consistent with the isolating effect of SiO_2 observed in Figure 5d. Nevertheless, up to 20 mol % SiO_2, these baseline values are

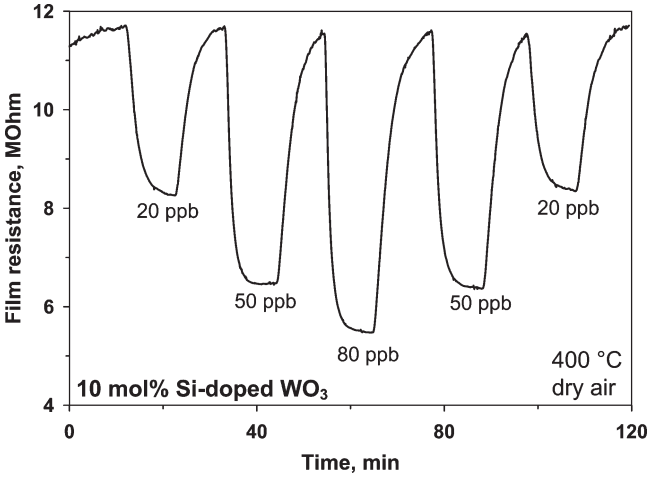

Figure 8. Resistance of 10 mol % Si-doped WO_3 sensor exposed to different ultra low acetone concentrations (20, 50, and 80 ppb) in dry air at 400 °C.

sufficiently small for integration in portable micro gas sensors.[16] The sensor response to 600 ppb acetone (Figure 7b, diamonds) increases from 1.6 to 4.6 with increasing Si content from 0 to 10 mol %. Increasing further, however, the Si content to 40 mol % reduces the sensor response down to practically zero. The optimal Si doping at 10 mol % is consistent with that (at 6 mol % or 2.5 wt % Si content) for Si-doped SnO_2 gas sensors[18] and is attributed to the progressive formation of dielectric, inert SiO_2 domains that isolate the gas-sensitive WO_3 crystallites with increasing Si content.

The sensor response in dry air of these optimally Si-doped WO_3 nanoparticles to 600 ppb acetone (Figure 7b, diamonds and 10 mol % Si content) is 4 times higher than that of Cr-doped WO_3 ones.[11] The response to acetone reaches a maximum at 10 mol % Si content, whereas that to ethanol (Figure 7b, triangles) or water vapor (circles) remains nearly constant up to 20% Si content. Therefore, the ratio between the response to acetone and that to ethanol or water vapor (e.g., selectivity to acetone over ethanol or water vapor) is increased from 1.7 and 3 to 4.7 and 10.4, at 0 and 10 mol % Si content, respectively. Furthermore, the acetone selectivity against 600 ppb ethanol or 20% rh (or 0.47×10^7 ppb) is also increased by Si doping up to 20 mol %. Here, this high selectivity to acetone is attributed to the large content (87 wt %) of the acentric ε-phase obtained and stabilized by Si doping.

The high sensitivity to acetone of the 10 mol % Si-doped WO_3 films allows detection of acetone traces (< 100 ppb) with remarkable signal-to-noise ratio. Figure 8 shows the resistance of a 10 mol % Si-doped WO_3 sensor in dry air and with 20, 50, and 80 ppb acetone at 400 °C. During injection of 20 ppb acetone, the film resistance is decreased from 11.7 to 8.3 MOhm that corresponds to a sensor response of 0.4. After flushing with pure air, the baseline is recovered within few minutes. This high response and signal-to-noise ratio allows to clearly distinguish between small acetone concentration increases (e.g., 50 and 80 ppb) always recovering the baseline. Detection of such low concentration of acetone has not been

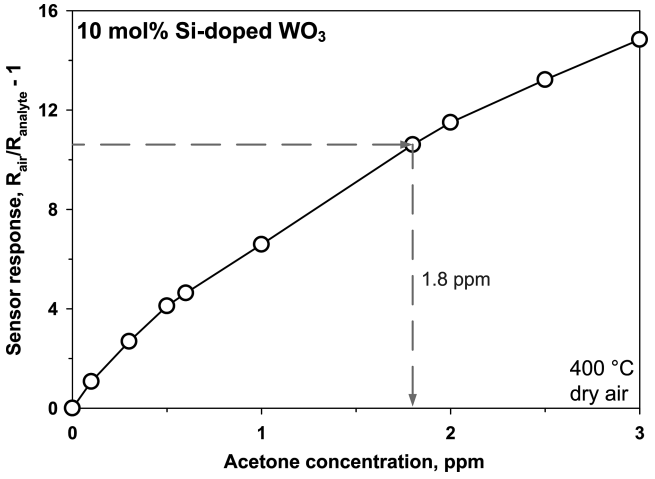

Figure 9. Calibration line for acetone detection (0−3 ppm) of a 10 mol % Si-doped WO_3 sensor in dry air at 400 °C. The steep difference, 6 and 10.5, in sensor response between 1 and 2 ppm, respectively, of acetone facilitates diagnosis of diabetes by breath analysis similar to that seen at realistic relative humidity conditions.[35]

reported for chemo-resistive gas sensors yet. This represents a key step toward the utilization of metal-oxide detectors in breath analysis as has been shown also for more realistic conditions (~ 90% rh).[34,35]

(34) Ferrus, L.; Guenard, H.; Vardon, G.; Varene, P. *Respir. Physiol.* **1980**, *39*, 367–381.
(35) Righettoni, M.; Tricoli, A.; Pratsinis, S. E. *Anal. Chem.* **2010**, in press DOI:10.1021/ac902695n.

Figure 9 shows the calibration line in dry air at 400 °C for the 10% Si-doped WO_3 sensor. The sensor response to acetone was below 6 at about 1 ppm and above 10.5 at about 2 ppm. This 43% difference in sensor response could allow precise diagnosis of diabetes by breath analysis. Even though this calibration line does not take into account the high relative humidity in the human breath, this difference is similar to that seen at realistic (90% rh) conditions.[35]

Conclusions

In conclusion, pure and Si-doped WO_3 nanoparticles have been made, directly deposited and in situ stabilized onto sensor substrates. Doping with Si increased the acetone-selective ε-WO_3 phase from 72 to 100 wt %. Furthermore, optimal (10 mol %) Si doping stabilized up to 87 wt % the ε-phase content at 500 °C while preventing grain and crystal growth. As a result, the acetone selectivity and response were increased allowing detection of acetone down to 20 ppb with extremely high signal-to-noise ratio by a cost-effective, solid-state detector that could be easily integrated in micro gas sensor systems.

Acknowledgment. Financial support was provided by CCMX, Nanoprim, and European Space Agency and the Swiss National Science Foundation, grant 200021_130582/1. We acknowledge stimulating discussions with Prof. P. Gouma (SUNY Stony Brook) and thank Dr. F. Krumeich (EMEZ, ETH Zurich) for the microscopic analysis.